

## Sediment transport in a restored, river-influenced Pacific Northwest estuary

Daniel J. Nowacki<sup>\*</sup>, Eric E. Grossman

*U.S. Geological Survey, Pacific Coastal and Marine Science Center, Santa Cruz, CA 95060, USA*

### ARTICLE INFO

#### Keywords:

Estuary restoration  
Sediment transport  
Tidal wetland  
Landslide

### ABSTRACT

Predicting the success of future investments in coastal and estuarine ecosystem restorations is limited by scarce data quantifying sediment budgets and transport processes of prior restorations. This study provides detailed analyses of the hydrodynamics and sediment fluxes of a recently restored U.S. Pacific Northwest estuary, a 61 ha former agricultural area near the mouth of the Stillaguamish River in Washington, USA. Water level, flow velocity, and suspended-sediment concentration (SSC) were measured between 21 March 2014 and 1 June 2015 at breaches excavated in the former flood-protection levee to determine transport patterns and the net sediment budget of the restoration area. SSC within the restoration area was primarily controlled by SSC variability of the nearby main stem Stillaguamish, but coastal processes also played a major role in sediment delivery. Fluvial sediment loading was dominated by runoff events associated with rainfall that lasted hours to a few days. Additionally, the 22 March 2014 SR 530 (Oso) landslide elevated sediment supply to the restoration area and coastal region for several weeks, indicating the importance of distal geomorphic events to coastal sediment budgets in small mountainous river systems. Sediment fluxes were controlled by river SSC and tidal dynamics, which set the quantity of water transported into the restoration area. Peak water discharge at the restoration area was about 12% of the river discharge, and peak sediment flux at the restoration area was about 5% of the river sediment discharge, although net sediment import was <1% of the total river load. Although sediment was imported to the restoration area, and inferred rates of accretion appear sufficient to keep pace with present rates of local sea-level rise, full recovery is challenged by significant lost grade from historical subsidence and will likely take decades to centuries. These results have implications for estuary restoration planning globally and indicate the importance of understanding coupled fluvial–coastal processes.

### 1. Introduction

Estuarine wetlands worldwide are at risk of extensive loss due to sea-level rise, and a quantitative understanding of coastal sediment budgets remains a principal data gap limiting their recovery and our ability to predict their fate (Neckles et al., 2002; Kirwan and Megonigal, 2013). Degradation from land-use activities including flood protection and conversion to agriculture has reduced the connectivity of wetlands to their sediment sources and has often led to land subsidence. As a result, significant additional sediment is required to recover lost elevation suitable for marsh habitat, in addition to that needed to mitigate potential drowning from sea-level rise. Furthermore, limited understanding of factors contributing to sediment transport in restored coastal ecosystems, including coupled fluvial–tidal processes, restricts successful adaptive management outcomes.

The international inland waterway known as the Salish Sea, which includes Puget Sound, the Strait of Juan de Fuca, and the Strait of Georgia, has experienced extensive loss of estuarine wetlands over the past several decades (Bortleson et al., 1980; Simenstad et al., 2011).

Some of the loss is attributable to agricultural reclamation, which can result in subsidence of up to 1–2 m relative to nearby coastal lands. This loss has prompted resource managers to identify and implement large-scale habitat restoration efforts across the region. One requirement of such restorations is to enable sufficient sediment import to recover lost grade and allow growth of desired marsh vegetation at a sufficient rate to mitigate sea level rise (e.g., Kirwan and Megonigal, 2013). Because of the high cost per unit area of marsh restorations, it is important to quantify the successes of such efforts (Ganju, 2019). Key metrics of successful ecosystem restoration efforts include sediment characteristics like accretion rate and elevation (Neckles et al., 2002), because post-restoration rebuilding of sediment depends on inorganic sediment flux and deposition rates adequate for the desired geomorphology and vegetation of the restoration area (Boumans et al., 2002), as well as organic matter accumulation (Nyman et al., 2006). Restoration success is possible; a study of 15 restored, previously leveed salt-marsh sites in San Francisco Bay showed that sufficient sediment supply and tidal exchange enabled relatively rapid establishment of vegetation in these

<sup>\*</sup> Corresponding author.

E-mail address: [dnowacki@usgs.gov](mailto:dnowacki@usgs.gov) (D.J. Nowacki).

<https://doi.org/10.1016/j.ecss.2020.106869>

Received 20 March 2020; Received in revised form 13 May 2020; Accepted 29 May 2020

Available online 30 May 2020

0272-7714/Published by Elsevier Ltd. This is an open access article under the CC BY license (<http://creativecommons.org/licenses/by/4.0/>).

restored areas (Williams and Orr, 2002). Levee breaching can be an effective restoration strategy leading to sufficient sediment accumulation to match present-day subsidence and sea-level rise rates, though ability to match increased future rates is uncertain (Van Der Deijl et al., 2018).

River-influenced wetlands are widespread. On the U.S. west coast, the rivers servicing these environments are often small mountainous rivers, which have been identified for their outsized contribution to worldwide sediment delivery to the ocean (Milliman and Syvitski, 1992). Sediment is delivered to the coastal zone via one or more river distributary channels, and to wetlands near river mouths via tidal channels; the number and characteristics of these channels are often anthropogenically modified. The suspended-sediment concentration of the riverine source and the distance of the river mouth from nearby marsh wetlands are both major factors in the sedimentary dynamics of the marsh (Friedrichs and Perry, 2001). If the connectivity between the riverine sediment source and the area of desired restoration and sediment accumulation is sufficient, the chances of a successful restoration may increase. Indeed, channel placement and location have been shown to be key to successful wetland restorations (Coats et al., 1989), and restorations can be enhanced with different breach configurations to increase sediment supply to the restored area (Van Der Deijl et al., 2018). Irrespective of breach placement, dike removal can improve conditions in locations outside (i.e., seaward) of the diked area (Hood, 2004). At a minimum, restoration efforts must consider the interaction of physical processes and morphodynamics to ensure the greatest likelihood of success (Williams and Faber, 2001).

In this paper we analyze data collected over the period March 2014–June 2015 at a restored former agricultural wetland area near the mouth of a small mountainous river in the Salish Sea. We describe the typical tidal and seasonal hydrodynamics and sediment dynamics of the system and how they relate to the computed water and sediment fluxes. Mechanisms that serve to increase these fluxes are considered, including the role of a catastrophic landslide that took place during the monitoring period. A sediment budget for the restoration area is computed and placed in context of other estimates for the region.

### 1.1. Study area

Port Susan is the receiving basin of the Stillaguamish River in Washington, USA (Fig. 1). Part of the greater Salish Sea estuary, Port Susan connects to the main basin of Puget Sound via Possession Sound to the south, and to Skagit Bay to the north via the much smaller conduits of South Pass, West Pass, and Davis Slough. The Stillaguamish River is undammed and drains 1800 km<sup>2</sup> of the northern Cascade Range and Puget Lowland and has a mean annual discharge of 85 m<sup>3</sup> s<sup>-1</sup>. Its primary distributary channel is Hat Slough; before about 1900 its primary distributary was the Old Stillaguamish Channel, which today is a tidal slough during low flow and a conduit for a fraction of the river discharge during high flow. Port Susan is mesotidal, with a mean tidal range of 2.3 m. During winter, Port Susan can receive considerable wave energy from predominantly south-southeast storm winds. During summer, winds and waves tend to be quiescent. Stillaguamish River discharge peaks in November through March under the influence of winter storms, and maintains relatively high flows during the spring freshet through May. Discharge is at a minimum in July, August, and September. Sediment discharge of the Stillaguamish is greatest in November–March. The Stillaguamish is an important salmonid rearing ground, and land-use changes including agricultural diking have led to large losses in off-channel salmon habitats (Pess et al., 2003).

In 2012 the Nature Conservancy restored 61 ha of diked and drained agricultural land at the mouth of Hat Slough. Numerical modeling carried out by Yang et al. (2010) suggested that removal of the dike would improve tidal flushing, increase the area exposed to freshwater, and support growth of four desired habitat types in the restoration area, which had been diked since the 1950s. Subsidence of up to 1 m occurred while the area was used for agricultural purposes. The

elevation of the former agricultural area, referred to in this paper as the marsh platform, is 1.4–1.7 m NAVD88. Dikes and levee-control structures along the north, west, and southern borders of the area were removed as part of the restoration; the elevation of the lowered levee is 2.1–2.6 m NAVD88. Additionally, two breaches, herein known as PSB1 and PSB2, were partially excavated through the former levees (Fig. 1) to encourage sediment exchange to, and accumulation within, the restoration area. Both breaches connect to channels which incise the marsh platform. The breaches are oriented to the west, away from the river, and are located toward the northern end of the restoration area. PSB1, the northern breach, was the largest and was where the time-series data presented in this work were collected. The breach was about 25 m in width and 2.5 m in depth at the thalweg. The PSB2 breach was about 12 m in width and ~1 m deep at the thalweg; cross-sectional data were collected here, as described in Section 2. Both breaches are fed from a ~20 m wide channel paralleling the western border of the restoration area, connecting to Hat Slough at the south and Port Susan to the north.

The data presented in this paper include effects from a catastrophic landslide which occurred 21 h after monitoring began at the restoration site. On 22 March 2014 17:37 UTC, a landslide mobilized approximately  $8 \times 10^6$  m<sup>3</sup> of material near the town of Oso, Washington, 62 river km upstream of the mouth of the Stillaguamish and the restoration site. The landslide caused 43 fatalities, destroyed 49 homes and structures, closed a stretch of Washington State Route 530 (SR 530), and temporarily blocked the North Fork of the Stillaguamish River. Extensive details about the influence of the landslide on the morphology of the nontidal Stillaguamish are available in Anderson et al. (2017b).

## 2. Methods

A combination of continuous and discrete measurements of water level, flow velocity, and turbidity were made from 21 March 2014 to 1 June 2015. A SonTek Argonaut-SW profiling velocity meter was deployed near the bed in the PSB1 breach thalweg and measured flow velocity and water level. Turbidity was measured by a collocated FTS Ltd. DTS-12 turbidity sensor.

In addition to measurements in the breach, we use discharge and SSC data from USGS stream gauge 12170300, located on Hat Slough near the town of Stanwood, WA (Fig. 1). PSB1 SSC was computed by using the turbidity-to-SSC rating for fine sediment derived at the Stanwood gauge (Anderson et al., 2017a):

$$C = 3.395 T^{0.832},$$

where  $T$  is turbidity and  $C$  is SSC. Wind data were obtained from the Arlington Municipal Airport, located approximately 16 km east of the study site. All times are in UTC. We use the convention of positive values representing ebbs and negative values representing floods.

### 2.1. Computation of water and sediment fluxes

We derived stage-to-area and index-velocity-to-mean-velocity relationships (Ruhl and Simpson, 2005) to determine water and sediment fluxes through the breaches (Fig. 2). Cross-sectional discharge measurements were made on 28 March, 16 April, 18 May, and 29 May 2014, and concurrently at PSB2 on 29 May 2014. The relationship between the velocity measured by the fixed instrument ( $v_i$ ) and the PSB1 mean channel velocity ( $v_m$ ) is

$$v_m = (0.639 \pm 0.023) v_i + (0.015 \pm 0.019), r^2 = 0.97. \quad (1)$$

Discharge measurements conducted concurrently at PSB1 and PSB2 on 29 May 2014 enable computation of the relative discharge of both breaches (Fig. 2). PSB2 discharge was approximately 42% that of PSB1 discharge:

$$Q_{PSB2} = (0.419 \pm 0.009) Q_{PSB1} - (0.579 \pm 0.320), r^2 = 0.99. \quad (2)$$

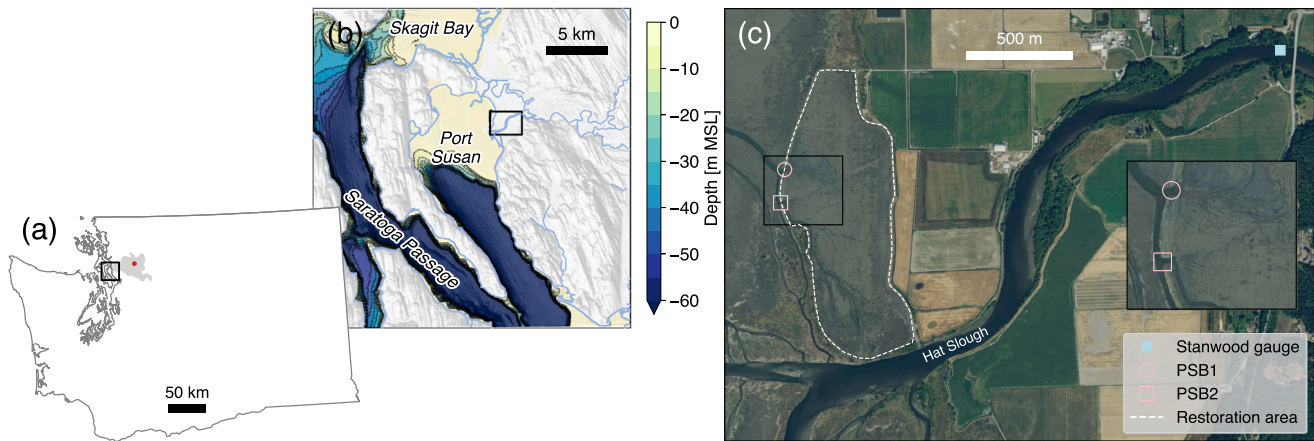


Fig. 1. (a): Map showing Washington State, Port Susan region (black rectangle), Stillaguamish River watershed (gray shading), and location of SR 530 landslide (red dot). (b): Map showing study area (black rectangle) in relation to Port Susan and surrounding region. (c): NAIP orthophoto showing study area and location of the PSB1 and PSB2 breaches, the Stillaguamish River gauge at Stanwood, WA (USGS 12170300), and the restoration area. Inset shows enlargement of the breach area.

A relationship between measured water level and cross-sectional area is used to compute the total water discharge by multiplying area by  $v_m$ . The relationship is straightforward when water level is below the former levee elevation, but is more challenging to determine when water level is higher than that elevation. We accomplished this task in several steps. The stage–area relationship of the PSB1 breach for water level lower than the levee elevation was computed from the ADCP cross-sectional measurements. This area was scaled to include the additional discharge provided by PSB2 following Eq. (2). For water levels below the levee elevation, this representation of area was multiplied by  $v_m$  to produce the water discharge  $Q$ .

When water levels were above the levee, we determined an effective levee length to add to the breach area. A combination of RTK-GPS measurements on the levee, airborne lidar, and imagery from the DigitalGlobe WorldView-2 satellite was used to estimate the effective length of levee inundation for a given water level by correlating Stillaguamish River water levels to levee inundation length at the time of image capture. The effective levee length for a given water level was multiplied by the corresponding water depth above the levees to produce the overtopped area. Because velocity was only measured within the breach, and flow velocity was likely slower in the shallower regions above the levee, we scaled the channel velocity measurements applied to the overtopped areas using the Manning equation by computing the ratio of the depth over the levees to the depth in the breach:

$$\left( h_{\text{levee}}^{2/3} \right) / \left( h_{\text{breach}}^{2/3} \right).$$

Sediment flux was computed by multiplying the discharge by the SSC calculated from the turbidity–SSC relationship and turbidity time series assuming a well-mixed water column.

Computing sediment fluxes in tidal environments is challenging, and it is important to estimate the errors involved to develop defensible determinations of net sediment flux and, subsequently, evaluate restoration success (Shellenbarger et al., 2013). Because of the several sources of error in measuring velocity, cross-sectional area, and SSC, we estimated uncertainty bands around the computed flux values, which are indicated in the ensuing text and figures. Details of the error analysis are given in Appendix.

### 3. Results

#### 3.1. Hydrodynamics and SSC

Tides were mixed semidiurnal; tidal ranges spanned 0.9 to 2.5 m over the deployment at the breach, which corresponded to breach thalweg depths of 0.6 to 3.9 m. Floods were generally stronger than

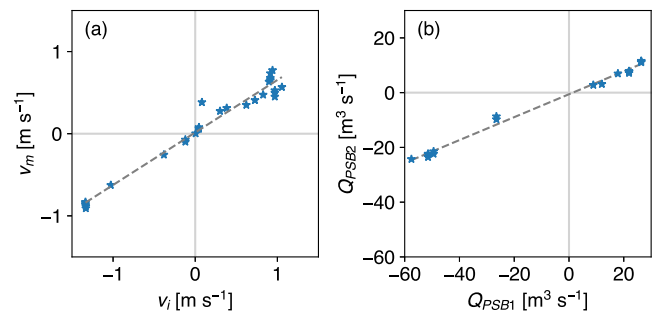


Fig. 2. (a): Relationship between index velocity and mean-channel velocity for PSB1. (b): Relationship between PSB1 and PSB2 water discharge. Regressions are given in Eqs. (1) and (2).

ebbs, with 95th-percentile values of  $0.69 \text{ m s}^{-1}$ , compared to  $0.59 \text{ m s}^{-1}$  on ebbs; ebbs generally were longer than floods and accounted for about 54% of the deployment time.

Mean PSB1 SSC was  $118 \text{ mg L}^{-1}$ . There was considerable tidal, storm, and season-scale variability in SSC; 90% of the values were between 12 and  $432 \text{ mg L}^{-1}$ , compared to a mean of  $179 \text{ mg L}^{-1}$  and range of 10 to  $628 \text{ mg L}^{-1}$  at Stanwood.

#### 3.1.1. Typical tidal dynamics

In order to describe the differing timescales of variability, we consider four representative tidal cycles from July (Fig. 3), which reveal a complex relationship between water level, velocity, and SSC at PSB1. PSB1 water levels follow a mixed semidiurnal tide with maximum tidal range of approximately 2.5 m. Stanwood water levels are similar to those at PSB1, although they are slightly elevated, given that gauge's location farther upstream, and have less-extreme lows, owing to the river's baseflow.

As water level rises from low slack water, flow velocity increases modestly, and then sharply increases as the water level exceeds the marsh-platform elevation, with maximum velocity approaching  $1 \text{ m s}^{-1}$ . This geomorphically controlled flow behavior is consistent with other tidal environments like tidal flats and salt marshes, which exhibit flow surges or pulses when the water level is near the flat elevation (e.g., Myrick and Leopold, 1963; Boon, 1975). During the ebb, flow velocity gradually builds to more than  $0.5 \text{ m s}^{-1}$  as the platform drains and rapidly decreases after the platform has emptied. In contrast to the strongly tidal dynamics at PSB1, discharge at Stanwood is nearly always downstream, although reversal does occur on the maximum flood during this period of low summer flow.

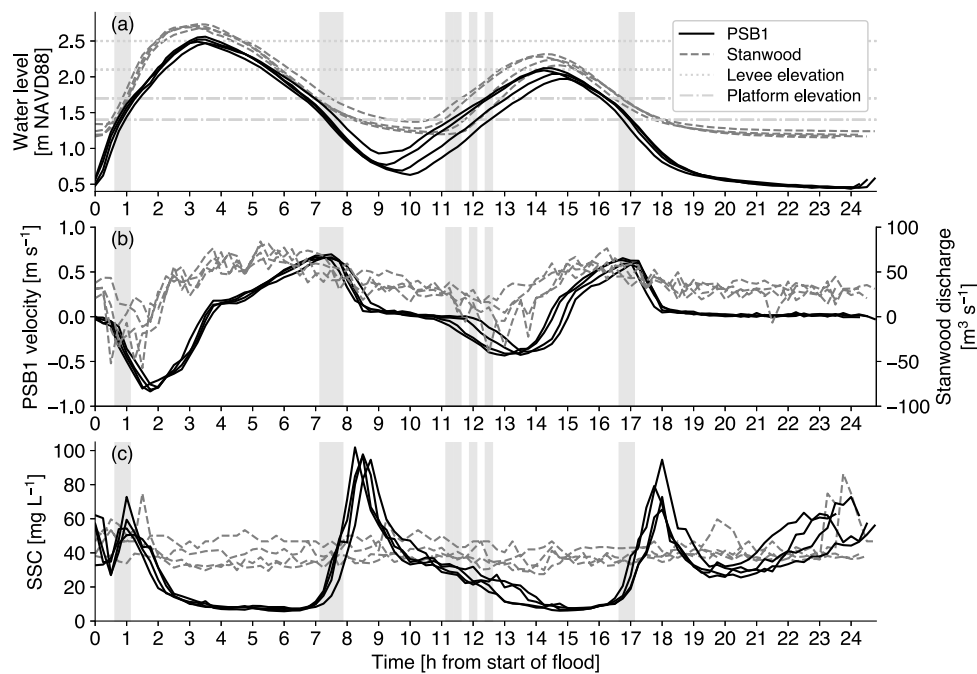


**Fig. 3.** Time series of (a) water level, (b) velocity, and (c) SSC at PSB1, and water level, discharge, and SSC at Stanwood, for four tidal cycles (26–30 July 2014). Gray vertical lines indicate times when PSB1 water level is within 5 cm of the marsh-platform elevation. Horizontal dotted lines in (a) indicate former levee elevation range; horizontal dash-dotted lines indicate marsh-platform elevation range. Maximum SSC during ebb occurs at the end of the ebb as water drains from the restoration area. A gradual increase in SSC is seen during extended low-water periods.

PSB1 SSC is relatively high on the maximum flood as water level passes the marsh-platform elevation, but begins to decrease prior to maximum velocity, and continues its decline as velocity wanes toward high slack water. SSC remains minimal on most of the ebb, and does not increase appreciably until water level is below the marsh-platform elevation, as flow velocity reaches its minimum. SSC continues to decay as currents switch to flood after this higher low water period. On the lesser flood, the peak in flow velocity is smaller, without a corresponding increase in SSC. On the following ebb, another sharp increase in SSC occurs after water level drops below the platform elevation, and SSC gradually increases throughout the elongated low-water period, potentially from delivery of turbid water as the marsh platform continues to drain. Throughout the deployment, SSC was often greatest during a given tidal cycle during extended low-water periods which occurred during lower-low tides under spring-tide conditions.

In contrast to the highly variable range in PSB1 SSC throughout the tidal cycle (~10–100 mg L<sup>-1</sup>), SSC at Stanwood was relatively stable without clear patterns related to tidal ebbs or floods, remaining between 30–50 mg L<sup>-1</sup>.

### 3.1.2. Dynamic influences and longer-term trends

At timescales longer than a tidal cycle, SSC patterns at PSB1 are strongly controlled by conditions in the Stillaguamish River (Fig. 4). PSB1 tidal-average SSC is highly correlated with Stanwood SSC ( $r^2 = 0.86$ ; Fig. 4a), suggesting that the mean, ambient SSC is determined by delivery from the Stillaguamish River. SSC at PSB1 was generally less than at Stanwood, potentially because energetic conditions in the Stillaguamish River main stem are more effective at maintaining sediment in suspension and sediment may settle out of suspension before reaching the breach. Exceptions from the strong correlation between SSC measured at Stanwood and PSB1 are found in the six days immediately following the SR 530 landslide (Section 4.1), when SSC was much greater at Stanwood than at PSB1 as the landslide sediment pulse propagated downstream.

As described in the previous section, PSB1 SSC variability within a tidal cycle is largely determined by water level relative to the marsh-platform elevation (Fig. 3). Similarly, across longer timescales representing a greater range of Stanwood SSC values, PSB1 SSC varies with

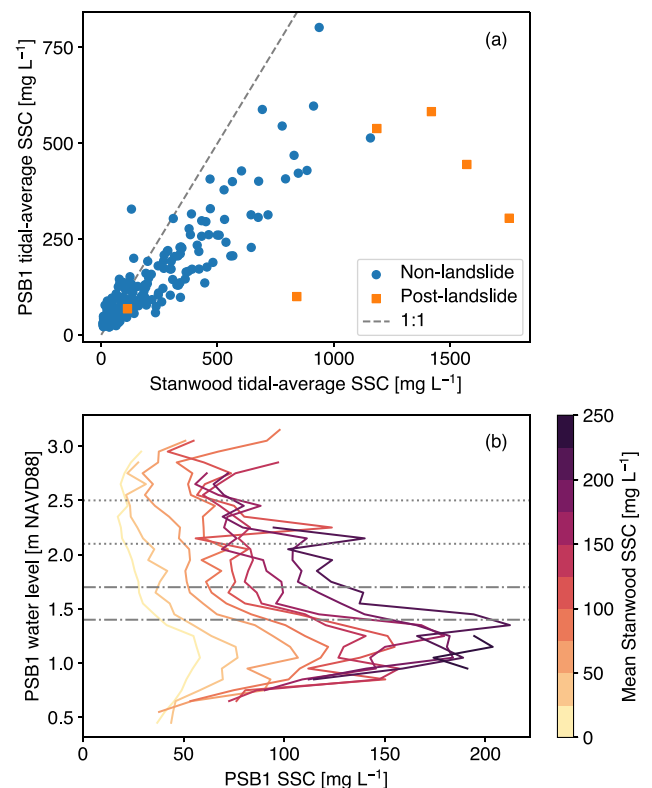


**Fig. 4.** (a): Tidally averaged Stanwood and PSB1 SSC ( $r^2 = 0.86$ ). Note outliers from the six days immediately following the SR 530 landslide. (b): Bin-averaged PSB1 SSC plotted against a range of binned water levels and mean Stanwood SSC values. Horizontal dash-dotted lines indicate marsh-platform elevation range; horizontal dotted lines indicate former levee elevation range. Note greater SSC for water levels below the platform elevation.

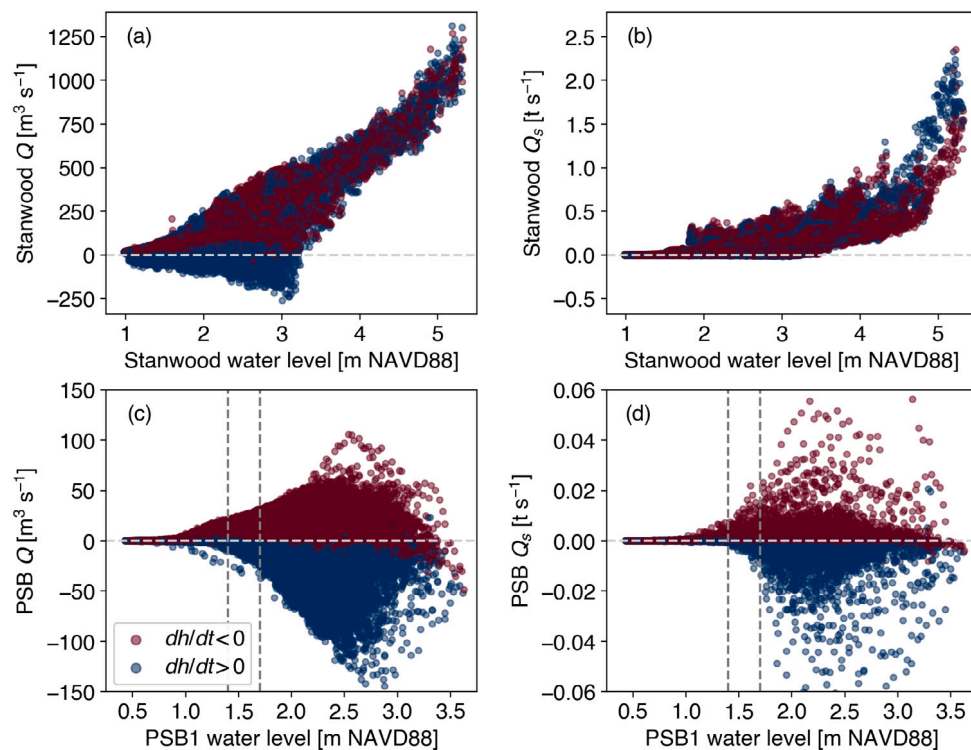


Fig. 5. Water and sediment discharge as a function of water level, colored by water level gradient (roughly interpreted here as flooding or ebbing conditions) at (a)–(b) Stanwood and (c)–(d): PSB1. Vertical dashed lines in (c) and (d) indicate elevation range of the salt-marsh platform.

water level and is greatest when water level is lower than the elevation of the marsh platform (Fig. 4b). Variation with water level is shifted on a mean SSC value set by a Stillaguamish-derived background concentration. The relationship between Stanwood and PSB1 SSC is less-tightly coupled when water levels are high. Offshore mixing of Stillaguamish discharge with less-turbid marine water, loss via seaward advection, or sediment settling at offshore locations reduces concentrations of the water delivered back to the restoration area during flood tides at higher water levels.

Wind-wave resuspension of sediment, both within the restoration area and particularly over the tidal flats to the west, is likely, but the co-occurrence of wind events and river flooding makes it challenging to disentangle these two signals. Sediment resuspension by wind may be an important additional component in the sediment budget, but the data collected in this study do not enable detailed analysis of the effects of wind.

### 3.2. Water and sediment fluxes

The dynamics of the Stillaguamish River are crucial to the SSC and sediment flux at the restoration area. Here we contrast water- and sediment-flux dynamics within the Stillaguamish River and at the restoration area. As described previously, tidal-average Stanwood SSC is highly correlated with tidal-average PSB1 SSC (Fig. 4a). The relationships between restoration-area and Stillaguamish water and sediment fluxes are more complex (Fig. 5). When Stanwood water level is above about 3.5 m NAVD88, water level is a robust indicator of water discharge, similar to most non-tidal rivers (Fig. 5a). Tidal fluctuations limit the utility of using water level to predict Stanwood discharge for water levels lower than about 3.5 m. Positive temporal water-surface gradients ( $dh/dt$ ) are required for flood (upstream) discharge at Stanwood, although a positive  $dh/dt$  may occur even when discharge is oriented downstream. Despite measurable upstream water flux at Stanwood, upstream sediment flux is negligible. At Stanwood, upstream water flux represents about 2% of the net discharge, but upstream

sediment flux represents only 0.1% of the net sediment discharge, as nearly all sediment transported downstream past Stanwood is lost to Port Susan and never re-imported upstream to this location (Fig. 5b).

In contrast to dynamics on the Stillaguamish, restoration-area water discharge is much more equally distributed between flood and ebb, although floods tend to be more intense than ebbs (Fig. 5c); here the water-surface gradient is a reliable indicator of flux direction. Restoration-area sediment fluxes are also strongly bidirectional (Fig. 5d). At the restoration area, both water and sediment fluxes are greatest at water levels above 2.5 m, the approximate elevation of the former levee; this increase is driven by the large effective area when water level is above the levee. The greatest unit-width water and sediment fluxes are observed at elevations between 1.75 and 2.25 m, i.e., above the elevation of the marsh platform.

Water- and sediment-flux magnitudes vary widely between Stanwood and the restoration area. The peak instantaneous restoration-area water flux, about  $160 \text{ m}^3 \text{ s}^{-1}$ , is approximately 12% of the peak river discharge of  $1300 \text{ m}^3 \text{ s}^{-1}$ ; similarly, the mean of the absolute value of the restoration-area discharge is about 12% of the Stanwood mean discharge. The sediment-transport capacity of the restoration area is much less than that of the river, likely because it exchanges a combination of river water, which may have lost much of its sediment via settling or advection along its circuitous path via tidal channels to the restoration area, and less-turbid marine water. The peak restoration-area sediment flux of  $0.11 \text{ t s}^{-1}$  is about 5% of the maximum Stanwood value of  $2.35 \text{ t s}^{-1}$ ; the mean of the absolute value of  $Q_s$  at PSB is  $0.0014 \text{ t s}^{-1}$ , just 3% of the mean Stanwood  $Q_s$  of  $0.047 \text{ t s}^{-1}$ .

### 3.3. Mechanisms increasing sediment flux

Storms increase restoration-area sediment transport via delivery from flooding of the Stillaguamish River. Although wind-wave sediment resuspension may occur, both over the tidal flats west of the restoration area and also within the restoration area, distinguishing this signal from that of the flooding Stillaguamish River is challenging. In

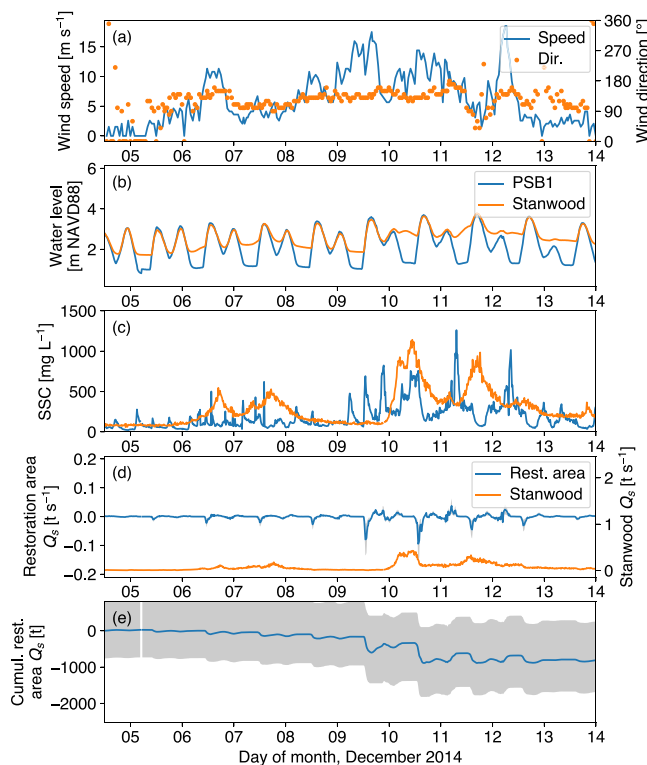


**Fig. 6.** Plot of (a) wind speed and direction, (b) PSB1 and Stanwood water level, (c) PSB1 and Stanwood SSC, (d) restoration area and Stanwood instantaneous sediment flux, and (e) cumulative restoration-area sediment flux during the December 2014 storm. Gray shading in (d) indicates uncertainty. This event resulted in sediment import to the restoration area.

addition to storms, enhanced PSB1 SSC values are associated with high flow velocities during spring tides, particularly on floods, suggesting local sediment resuspension.

Coastal storms generally result in sediment import to the restoration area. A storm during December 2014 (Fig. 6) is typical. During this storm, which had winds from the SE that peaked at more than  $15 \text{ m s}^{-1}$ , a combination of sediment resuspension from spring-tidal flows and, later, moderately increased delivery from the Stillaguamish River, led to greater sediment fluxes in the restoration area. The combination of these mechanisms imported about 1 kt of sediment to the restoration area during this event (Fig. 6e). Despite the net sediment import, SSC was elevated on both floods and ebbs (Fig. 6c), and water fluxes increased on both flood and ebb tides.

Coastal storms and floods of the Stillaguamish River can also occasionally result in apparent sediment export from the restoration area, as occurred during a late-November 2014 storm. Flooding of the Stillaguamish River in excess of 2 m above the preexisting river stage (Fig. 7) led to inundation of the restoration area directly from the south, over the river-adjacent former levee top (Fig. 7b; see Fig. 1 for context). The former-levee elevation adjacent to Hat Slough is 3.0–3.4 m, higher than the former levee closer to the breaches. The direct delivery of highly turbid water via this flow path subsequently led to advection of this water mass out of the restoration area via the breaches over the ensuing tidal cycles. Local resuspension over the marsh platform also could have contributed to the observed sediment export. As measured at PSB1, approximately 1 kt of sediment was exported from the restoration area during this 5 day event (Fig. 7e). Despite the PSB1 observations, this event could still have resulted in net sediment import to the restoration area via deposition over the marsh platform not captured by these data; this possibility is discussed further in Section 4.2.

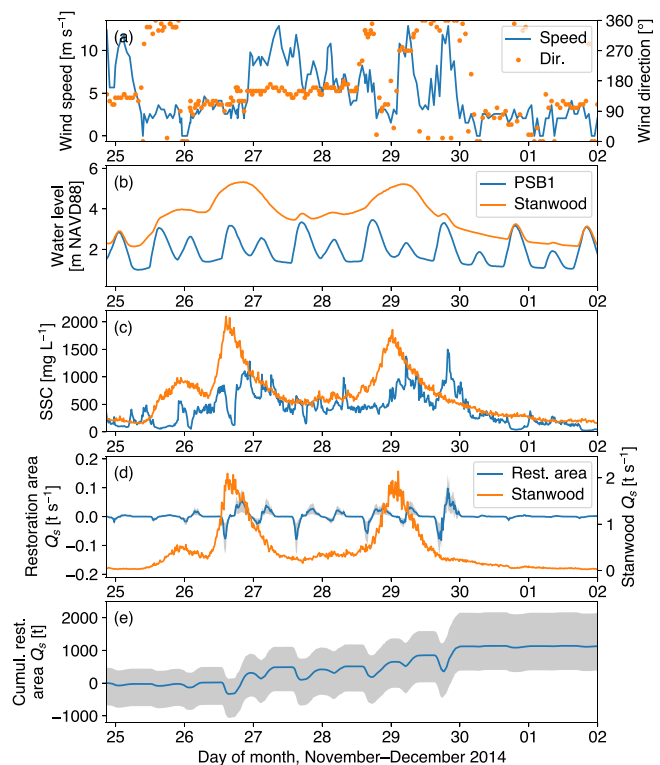


**Fig. 7.** Plot of (a) wind speed and direction, (b) PSB1 and Stanwood water level, (c) PSB1 and Stanwood SSC, (d) restoration area and Stanwood instantaneous sediment flux, and (e) cumulative restoration-area sediment flux during the November–December 2014 storm. Gray shading in (d) indicates uncertainty. This event resulted in apparent sediment export from the restoration area.

During spring tides, enhanced tidal velocities increase bed stresses and are associated with elevated SSC (Fig. 8). Particularly during floods, which tend to be stronger than ebbs, the minimum SSC increases with increasing bed stress. This is a primary way by which sediment concentrations can vary during periods of low Stanwood SSC. Local resuspension of sediment from the tidal flats west of the restoration area, and from within the feeder channels which connect the breaches to the tidal flats and the main stem Stillaguamish, is a likely mechanism by which this increase in SSC is accomplished. Indeed, meaningful tidal-scale variability in SSC is locally derived, because Stanwood SSC is not sensitive to tidal dynamics (Figs. 3, 6, 7).

## 4. Discussion

### 4.1. SR 530 landslide

The catastrophic SR 530 landslide was the largest sedimentary signal observed during this study. A combination of temporary blocking of the Stillaguamish and travel time of the sediment signal resulted in a measurable time lag between the landslide and its evidence in the lower Stillaguamish River and restoration area. An increase in sediment flux and SSC at the Stanwood gauge began at 24 March 2014 14:30, 44 h after the slide and 20 h after the river overtopped the slide deposit (23 March 2014 18:30; Magirl et al., 2015). This corresponds to a speed of about  $2.9 \text{ km h}^{-1}$  for the landslide sediment pulse to travel the 58 river km between the slide and Stanwood (Anderson et al., 2017b). At PSB1, the landslide signal arrived at 25 March 2014 06:00, about 16 h after its appearance at Stanwood. Assuming a shortest-path distance along the river channel from the Stanwood gauge to PSB1 of approximately 4.5 km, this corresponds to an average speed of about  $0.3 \text{ km h}^{-1}$ , about 10% of that between the landslide location and Stanwood. This

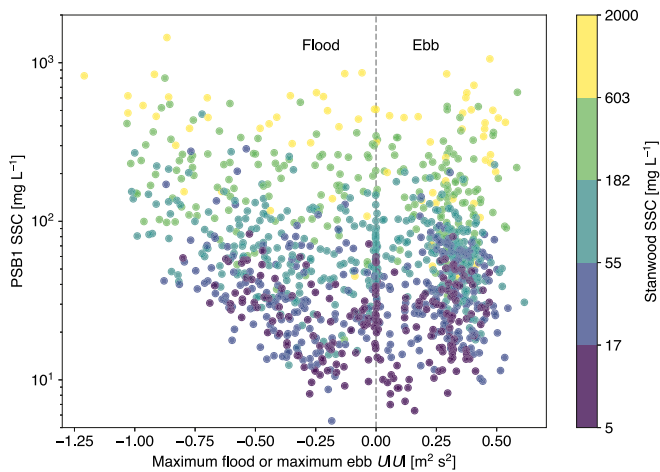


**Fig. 8.** Plot of  $U/|U|$  during maximum flood and maximum ebb versus PSB1 SSC. Points are colored by Stanwood SSC. Note log scales on y axis and color bar. The quantity  $U/|U|$  is directly related to bed stress under a quadratic drag equation.

much-reduced travel speed represents a lower bound as it assumes a shortest-path estimate. If the signal took a more circuitous path in the tidal cycles between its appearance at Stanwood and at PSB1, the effective travel speed would increase. Nevertheless, the slower propagation reflects the presence of tidal processes in the Stillaguamish estuary and Port Susan, and the greatly reduced hydraulic gradient between Stanwood and PSB1 compared to that of the upper river.

The initial landslide pulse delivered more than 500 t of sediment to the restoration area in a single tidal cycle on 26 March (Fig. 9). Over the ensuing three days, an additional  $\sim 300$  t, for a total of nearly 1 kt, was delivered. Although missing data limit our knowledge of dynamics on 29 March–3 April, extending the slope of the cumulative sediment flux over those days suggests a total of about 2 kt of sediment attributable to the landslide was imported to the restoration area between 26 March and 4 April, which is when the initial pulse from the landslide decayed at Stanwood. This landslide-associated value represents nearly 50% of the total sediment imported to the restoration area during the study (Section 4.2). Approximately 50% of the total sediment load at Stanwood from March 22 2014 to September 30 2014 was attributed to the landslide (Anderson et al., 2017b); this value decreased to about 30 percent of the total load for the period March 2014–September 2015. These values suggest that the landslide's influence was comparable on the main stem and in the restoration area.

Clear evidence of the SR 530 landslide at PSB1, more than 60 river km downstream of the landslide site, indicates both the immense magnitude of the event and also the importance of distal watershed processes to coastal sedimentary processes, coastal ecosystems, and shorelines reliant on sedimentation but vulnerable to the effects of sea-level rise. This importance is especially evident in coastal settings influenced by small, steep, and sediment-rich mountainous rivers.

#### 4.2. Sediment budget

Here we estimate the net sediment budget for the restoration area over the course of a year. First, we assume that the majority of sediment comes through the breaches and over the western former levees, and that conditions measured at PSB1 are representative of the entire restoration-area boundary. Water and sediment that enter the restoration area via pathways not represented by conditions at the breach (e.g., large river floods, as occurred during late November 2014) may not be accurately captured by this approach, leading to the potential for under- or overprediction. Nevertheless, the extensive temporal coverage of the data set presented here enables computation of the

sediment budget which can help assess restoration success and evaluate additional sediment resource and adaptation needs.

We estimate a net sediment import to the restoration area of 3.3–5.5 kt over the approximately 15 months of data collection, which corresponds to 2.6–4.3  $\text{kt y}^{-1}$  (Fig. 10). The 2014–2015 sediment discharge at Stanwood was approximately  $1.4 \times 10^3 \text{ kt y}^{-1}$  (Anderson et al., 2017a), which places it as the second-largest riverine sediment source to Puget Sound (Czuba et al., 2011). In this context, the  $\sim 3.5 \text{ kt y}^{-1}$  delivered to the restoration area represents about 0.2% of the total sediment discharge at Stanwood. The Stanwood fine suspended-sediment load ( $<63 \mu\text{m}$ ) was approximately  $800 \text{ kt y}^{-1}$ ; similarly, the flux of sediment into the restoration-area is only about 0.5% of that value. A prior estimate of the Stillaguamish River sediment discharge, based on measurements made in 1964–66, indicates a far smaller sediment load of about  $16 \text{ kt y}^{-1}$  (Downing, 1983). Our restoration-area estimate is about 15%–30% of that value. In this study, the great differences in water and sediment fluxes between the restoration area and Stillaguamish River do not indicate that the restoration area imports one-quarter of what is transported in the river. Stillaguamish River sediment fluxes may have increased since the 1960s as a result of logging and other land-use changes; whether such changes could drive an approximately 100-fold increase is uncertain. An additional possibility is that increased sediment delivery from the SR 530 landslide (Section 4.1) could account for some of the differences among the studies. As mentioned previously, however, approximately 30% of the total sediment load at Stanwood during the study period March 2014–September 2015 was attributed to the landslide (Anderson et al., 2017b), suggesting that increased landslide sediment does not account for the differences in the measurements, and points to the possibility that the 1960s data were anomalously low for unknown reasons.

Our sediment budget is hampered by a lack of knowledge of circulation taking place within the restoration area. It is possible for water and sediment to enter the restoration area by flooding the southern levee adjacent to Hat Slough and exit via the breaches and western levee, as occurred during the November storm (Fig. 7). During that event, our observations suggest sediment export from the restoration area, even though it is likely some amount of the sediment delivered via overtopping of the river-adjacent levee was trapped within the restoration area before the remainder exited via the breaches. More subtle circulation dynamics such as sediment import via PSB1 and export via PSB2 may also occur, although our observations suggest similar behavior at both breaches (Fig. 2). Uncertainty of dynamics when the levees are overtopped is another source of potential error; levees were inundated about 12% of the time during the deployment.

#### 4.3. Comparison of measured sediment fluxes to SET and geochemical observations

The suspended-sediment fluxes can be converted to vertical sediment accretion with representative bulk density values and assumptions of sediment distribution. Using a bulk density of  $920 \text{ kg m}^{-3}$  within the restoration area (Poppe and Rybczyk, 2019) and assuming uniform sedimentation across the restoration area, we calculate an equivalent accumulation rate of 0.5–0.8  $\text{cm y}^{-1}$  (Fig. 10). Local relative sea-level rise at the NOAA Port Townsend tide gauge 30 km west of the study site is approximately  $0.19 \text{ cm y}^{-1}$ , suggesting that the restoration area is importing sufficient material to keep pace with sea-level rise. These rates may not be adequate, however, to counter regionally projected increased sea-level rise of 0.5–0.6  $\text{cm y}^{-1}$  (Miller et al., 2018).

By way of comparison to our values, we consider elevation change measured by Poppe and Rybczyk (2019), who used surface-elevation tables (SETs; Cahoon et al., 2002) at 21 locations across the Stillaguamish River estuary, within the restoration area and also at reference locations north and south of the river mouth. Between 2011 and 2018, the mean elevation change within the restoration area was  $2.74 \text{ cm y}^{-1}$ , nearly three times greater than the mean accretion rate of  $1.03 \text{ cm y}^{-1}$  in the

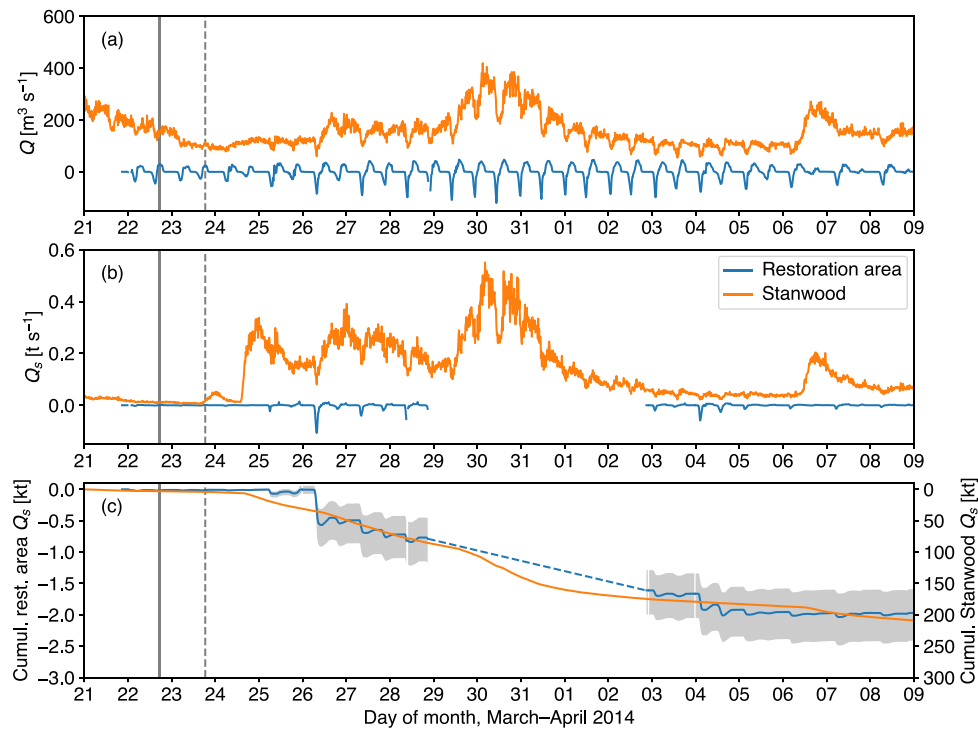


**Fig. 9.** Stanwood and restoration-area (a): water discharge, (b): sediment discharge, and (c): cumulative sediment discharge, before and after the SR 530 landslide. Note y-axis on right-hand side of (c) has been inverted for easier comparison between Stanwood and restoration-area fluxes. Shaded area in (c) indicates uncertainty. Solid vertical lines indicate time of landslide, 22 March 2014 17:37 UTC; dashed vertical lines indicate time when river overtopped the landslide deposit, 23 March 2014 18:30 UTC. Note increases in  $Q_s$  on 24 March at Stanwood and on 25 March at the restoration area.

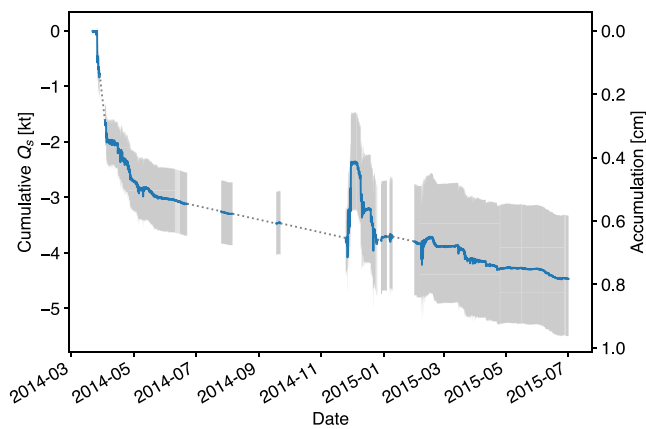


**Fig. 10.** Cumulative sediment discharge into the restoration area (negative values indicate sediment import) and estimated amount of vertical sediment accumulation. Shaded regions indicate uncertainty.

natural-marsh comparison sites. In addition to the SET results, [Poppe and Rybczyk \(2019\)](#) computed accumulation rates using the naturally occurring radioisotope  $^{210}\text{Pb}$ . Accumulation rates were  $1.57 \text{ cm y}^{-1}$  within the restoration area and  $0.60 \text{ cm y}^{-1}$  in the natural-marsh sites. The accumulation rates from the SET and radiochemical results are marginally larger than values inferred from our instrument observations. The differences could result from uneven sediment redistribution within the restoration area (i.e., the assumption of uniform sedimentation is invalid) and also the different time scales considered by each method. Further, the sediment-flux estimate reflects mineral accretion and does not account for vegetation influence on vertical accumulation. These paired results suggest that sediment accumulation throughout the region is sufficient to keep pace with present sea-level rise.

Using the accumulation values derived from our observations, the time required to regain the marsh elevation lost to subsidence during its period of agricultural use is of order 150–300 y; the SET and geochemical observations suggest a recovery time of 40–70 y. The time needed to recover this grade may lengthen under potential future increased rates of sea-level rise, although additional accommodation space provided by higher sea level could enable enhanced deposition.

#### 4.4. Future outlook and implications for this and other restoration efforts

The location and configuration of coastal habitat restorations are often set by external factors including land ownership, land use, and the potential for storm- and flood-risk modification resulting from the restoration. For example, restored tidal exchange may be limited within a restoration in order to reduce flooding risk to nearby residential or commercial areas. As a result, levee removal and breaches may not be placed in locations ideal for restoring processes that enable the most rapid habitat recovery possible. In the case of the Port Susan restoration, the breaches were placed far from Hat Slough and oriented away from its fluvial sediment source. [Fuller \(2018\)](#) hypothesized that such an orientation would lead to sediment bypassing of the restoration, lengthening the time required to achieve restoration success. Our results show that, despite this less-than-ideal breach placement with respect to the riverine sediment source, a solid connection between the dynamics in the Stillaguamish River and the restoration area was achieved. It is likely, however, that breach placement closer to Hat Slough would accelerate the delivery of sediment to the restoration and shorten the timescale of restoration success. Additionally, a considerable fraction of the observed sediment import during this study was a result of the anomalous SR 530 landslide; landslides are infrequent and unpredictable sources of sediment. The return to background rates of fluvial sediment loading is expected to reduce sediment delivery rates below those observed during this study and could slow progression toward full geomorphic and habitat recovery over the coming years.

This study suggests the importance in planning efforts of considering the complex relationship between a restoration area and its sediment sources. Sediment availability at the restoration area in the form of tidally averaged SSC was strongly controlled by the Stillaguamish River. Variability around this mean SSC level was additionally modulated by the geomorphic configuration of the restoration area within the tidal prism (Figs. 3 and 4) as well as local resuspension (Fig. 8). Remaining concerns for this site and estuaries more broadly include how future changes in the timing and magnitude of sediment delivery from fluvial sources, variability in storm intensity and character, and evolution of geomorphology and vegetation structure will interact and influence sediment import and retention. Assuming sufficient sediment supply, accelerated sea-level rise that increases accommodation space may enhance sedimentation, although changes in wave dynamics with higher water levels may increase wave erosion and sediment redistribution.

Estuary restoration efforts can benefit from improved understanding of the role of tidal and coastal processes in delivering sediment to restoration areas. Vulnerability associated with historical subsidence and the projected acceleration of sea-level rise suggest a need to enhance sediment delivery for marsh re-establishment and sustainability. A greater likelihood for restoration success may arrive via increased sediment retention from more direct river connections. In the restoration site studied here, channel reconnection along the south levee would allow for direct sediment input from the Stillaguamish main stem. Such a connection would promote greater sediment flux and likely lead to increased sedimentation, particularly of larger particle sizes more capable of elevating the subsided grade, as compared to the primarily fine material delivered by tidal processes through the existing breaches. Proximity to a significant fluvial sediment source is likely essential for the success of this area as well as many estuaries worldwide identified for recovery of wildlife populations and ecosystem services. Other proposed restoration efforts without a nearby source face a more uncertain future.

## 5. Conclusion

Measurements of hydrodynamics and sediment transport in a recently restored estuary and its dominant fluvial sediment source reveal factors that are rarely incorporated in coastal planning but that affect shoreline stability, flood risk management, and habitat restoration. Through analyses of flow characteristics and sediment transport, we constructed a quantitative sediment budget for a restored estuary and identified the importance of coastal processes in modulating the delivery of sediment from a river to its nearby restored marshes. Although sediment availability to the restoration area was strongly controlled by conditions in the nearby Stillaguamish River, net flux into the marsh was <1% of the river load. A large fraction of this load was delivered by the March 2014 SR 530 (Oso) landslide, indicating the importance of distal geomorphic processes in affecting estuarine dynamics and maintaining processes critical to shoreline stability in small mountainous river systems. The derived sediment budget of the restored marsh of 2.6–4.3 kt y<sup>-1</sup> is sufficient to counter present-day rates of sea level rise, but decades to centuries are likely required to recover ~1 m of lost grade associated with historical subsidence caused by agricultural diking. Future restoration efforts should consider the mechanisms of connectivity between a restoration area and its sediment source in order to maximize the likelihood of restoration success.

## CRedit authorship contribution statement

**Daniel J. Nowacki:** Writing - original draft, Writing - review & editing, Visualization, Data curation, Conceptualization, Methodology, Investigation. **Eric E. Grossman:** Writing - review & editing, Funding acquisition, Conceptualization, Methodology, Investigation, Project administration.

## Declaration of competing interest

The authors declare that they have no known competing financial interests or personal relationships that could have appeared to influence the work reported in this paper.

## Acknowledgments

This study was supported by the National Oceanic and Atmospheric Administration Restoration Center, Washington Department of Fish and Wildlife Estuary and Salmon Restoration Program, The Nature Conservancy, and the U.S. Geological Survey as part of the USGS Coastal Habitats in Puget Sound Project. We thank Chris Curran, Katherine Hancock, and Roger Fuller for their assistance in the field. Comments from two anonymous reviewers are gratefully acknowledged. Data presented in this study are available at <https://doi.org/10.5066/P9RK8H7X>. Any use of trade, firm, or product names is for descriptive purposes only and does not imply endorsement by the U.S. Government.

## Appendix. Error analysis

Nine constituents comprise the sediment flux, each with an associated error: (a) measured velocity; (b) slope and (c) intercept of regression between measured velocity and channel mean velocity; (d) measured water level; (e) slope and (f) intercept between measured water level and channel area; (h) measured turbidity; (g) coefficient and (i) exponent of regression between measured turbidity and SSC. The errors for (a), (d), and (h) were obtained from manufacturer documentation, and the regression errors were computed using standard statistical techniques (Table A.1). In this context, the sediment flux is defined as

$$Q_s = (ab + c)(de + f)(gh^i),$$

and the total error in  $Q_s$  is

$$\delta Q_s = \sqrt{\left(\frac{\partial Q_s}{\partial a} \delta a\right)^2 + \dots + \left(\frac{\partial Q_s}{\partial i} \delta i\right)^2},$$

where  $\delta a \dots \delta i$  are the errors associated with the constituent terms, following standard error-propagation methods (Taylor, 1997).

To determine whether the propagated error will significantly influence the results presented in this work, we derive the propagated error for the sediment flux. The total fractional sediment-flux error ( $\delta Q_s / |Q_s|$ ) varies depending on the magnitude of the constituent terms, but the peak of the fractional error distribution indicates 65% propagated error from all contributing terms  $a-i$ . The intercept of the regression between measured and channel-mean velocity represents the largest constituent error because its value is close to zero with a relatively large uncertainty. The propagated error for  $Q_s$ , computed by obtaining the 95th-percentile range of 1000 realizations of the error distribution is indicated with gray shading in Figs. 6, 7, 9, and 10. Although the propagated error increases uncertainty in the results, it does not meaningfully alter the conclusions drawn.

**Table A.1**  
Constituent and propagated fractional errors at PSB1.

Constituent	Error
$\delta a /  a $	0.03
$\delta b /  b $	0.01
$\delta c /  c $	1.29
$\delta d /  d $	0.05
$\delta e /  e $	0.51
$\delta f /  f $	0.11
$\delta g /  g $	0.37
$\delta h /  h $	0.05
$\delta i /  i $	0.07
$\delta Q_s /  Q_s $	0.65

## References

- Anderson, S.W., Curran, C.A., Grossman, E.E., 2017a. Suspended-sediment loads in the lower Stillaguamish River, Snohomish County, Washington, 2014–15. U.S. Geological Survey Open-File Report 2017-1066, p. 10. <http://dx.doi.org/10.3133/ofr20171066>.
- Anderson, S.W., Keith, M.K., Magirl, C.S., Wallick, J.R., Mastin, M.C., Foreman, J.R., 2017b. Geomorphic response of the North Fork Stillaguamish River to the State Route 530 landslide near Oso, Washington. U.S. Geological Survey Scientific Investigations Report 2017–5055, p. 85. <http://dx.doi.org/10.3133/sir20175055>.
- Boon, J., 1975. Tidal discharge asymmetry in a salt marsh drainage system. *Limnol. Oceanogr.* 20 (1), 71–80. <http://dx.doi.org/10.4319/lo.1975.20.1.0071>.
- Bortleson, G.C., Chrzastowski, M., Helgerson, A., 1980. Historical changes of shoreline and wetland at eleven major deltas in the Puget Sound region, Washington. U.S. Geological Survey Hydrologic Atlas 617, <http://dx.doi.org/10.3133/ha617>.
- Boumans, R., Burdick, D., Dionne, M., 2002. Modeling habitat change in salt marshes after tidal restoration. *Restor. Ecol.* 10 (3), 543–555. <http://dx.doi.org/10.1046/j.1526-100X.2002.02032.x>.
- Cahoon, D.R., Lynch, J.C., Perez, B.C., Segura, B., Holland, R.D., Stelly, C., Stephenson, G., Hensel, P., 2002. High-precision measurements of wetland sediment elevation: II. The rod surface elevation table. *J. Sediment. Res.* 72 (5), 734–739. <http://dx.doi.org/10.1306/020702720734>.
- Coats, R., Swanson, M., Williams, P., 1989. Hydrologic analysis for coastal wetland restoration. *Environ. Manag.* 13 (6), 715–727. <http://dx.doi.org/10.1007/BF01868311>.
- Czuba, J.A., Magirl, C.S., Czuba, C.R., Grossman, E.E., Curran, C.A., Gendaszek, A.S., Dinicola, R.S., 2011. Sediment load from major rivers into Puget Sound and its adjacent waters. U.S. Geological Survey Fact Sheet 2011-3083, p. 4. <http://dx.doi.org/10.3133/fs20113083>.
- Downing, J., 1983. *The coast of Puget Sound*. University of Washington Press, Seattle, Washington, p. 126.
- Friedrichs, C., Perry, J., 2001. Tidal salt marsh morphodynamics: a synthesis. *J. Coast. Res.* SI (27), 7–37, URL: <http://www.jstor.org/stable/10.2307/25736162>.
- Fuller, R.N., 2018. Port Susan Bay estuary restoration project final monitoring report. Technical Report, prepared for The Nature Conservancy.
- Ganju, N.K., 2019. Marshes are the new beaches: Integrating sediment transport into restoration planning. *Estuar. Coasts* 42 (4), 917–926. <http://dx.doi.org/10.1007/s12237-019-00531-3>.
- Hood, W.G., 2004. Indirect environmental effects of dikes on estuarine tidal channels: Thinking outside of the dike for habitat restoration and monitoring. *Estuaries* 27 (2), 273–282. <http://dx.doi.org/10.1007/bf02803384>.
- Kirwan, M.L., Megonigal, J.P., 2013. Tidal wetland stability in the face of human impacts and sea-level rise. *Nature* 504 (7478), 53–60. <http://dx.doi.org/10.1038/nature12856>.
- Magirl, C.S., Keith, M.K., Anderson, S.W., O'Connor, J.E., Aldrich, R., Mastin, M.C., 2015. Preliminary assessment of aggradation potential in the North Fork Stillaguamish River downstream of the State Route 530 Landslide near Oso, Washington. U.S. Geological Survey Scientific Investigations Report 2015–5173, p. 20. <http://dx.doi.org/10.3133/sir20155173>.
- Miller, I., Morgan, H., Mauger, G., Weldon, R., Schmidt, D., Welch, M., Grossman, E., 2018. Projected sea level rise for Washington state – A 2018 assessment. Technical Report, Prepared for the Washington Coastal Resilience Project, p. 24.
- Milliman, J.D., Syvitski, J.P.M., 1992. Geomorphic/tectonic control of sediment discharge to the ocean: The importance of small mountainous rivers. *J. Geol.* 100 (5), 525–544. <http://dx.doi.org/10.1086/629606>.
- Myrick, R.M., Leopold, L.B., 1963. Hydraulic geometry of a small tidal estuary. U.S. Geological Survey, <http://dx.doi.org/10.3133/pp422B>.
- Neckles, H.A., Dionne, M., Burdick, D.M., Roman, C.T., Buchsbaum, R., Hutchins, E., 2002. A monitoring protocol to assess tidal restoration of salt marshes on local and regional scales. *Restor. Ecol.* 10 (3), 556–563. <http://dx.doi.org/10.1046/j.1526-100X.2002.02033.x>.
- Nyman, J.A., Walters, R.J., Delaune, R.D., Patrick, W.H., 2006. Marsh vertical accretion via vegetative growth. *Estuar. Coast. Shelf Sci.* 69 (3–4), 370–380. <http://dx.doi.org/10.1016/j.ecss.2006.05.041>.
- Pess, G., Montgomery, D.R., Beechie, T.J., Holsinger, L., 2003. Anthropogenic alterations to the biogeography of Puget Sound salmon. In: *Restoration of Puget Sound Rivers*. University of Washington Press, Seattle, Washington, pp. 129–154.
- Poppe, K., Rybczyk, J., 2019. A blue carbon assessment for the Stillaguamish River estuary: Quantifying the climate benefits of tidal marsh restoration. Technical Report, Western Washington University, p. 19.
- Ruhl, C.A., Simpson, M.R., 2005. Computation of discharge using the index-velocity method in tidally affected areas. U.S. Geological Survey, p. 31. <http://dx.doi.org/10.3133/sir20055004>.
- Shellenbarger, G.G., Wright, S.A., Schoellhamer, D.H., 2013. A sediment budget for the southern reach in San Francisco Bay, CA: Implications for habitat restoration. *Mar. Geol.* 345, 281–293. <http://dx.doi.org/10.1016/j.margeo.2013.05.007>.
- Simenstad, C., Ramirez, M., Burke, J., Logsdon, M., Shipman, H., C, T., Toft, J.D., Craig, B., Davis, C., Fung, J., Bloch, P., Fresh, K.L., Campbell, S., Myers, D., Iverson, E., Bailey, A., Schkenger, P., Kiblinger, C., Myre, P., Gerstel, W., MacLennan, A., 2011. Historical change and impairment of Puget Sound shorelines. Technical Report, Puget Sound Nearshore Ecosystem Restoration Project, p. 289, URL: [http://www.pugetsoundnearshore.org/technical\\_papers/change\\_analysis.pdf](http://www.pugetsoundnearshore.org/technical_papers/change_analysis.pdf).
- Taylor, J.R., 1997. *An introduction to error analysis*, second ed. University Science Books, p. 327.
- Van Der Deijl, E.C., Van Der Perk, M., Middelkoop, H., 2018. Establishing a sediment budget in the newly created “kleine Noordwaard” wetland area in the Rhine-Meuse delta. *Earth Surf. Dyn.* 6 (1), 187–201. <http://dx.doi.org/10.5194/esurf-6-187-2018>.
- Williams, P., Faber, P., 2001. Salt marsh restoration experience in San Francisco Bay. *J. Coast. Res.* SI27, 203–211.
- Williams, P.B., Orr, M.K., 2002. Physical evolution of restored breached levee salt marshes in the San Francisco Bay estuary. *Restor. Ecol.* 10 (3), 527–542. <http://dx.doi.org/10.1046/j.1526-100X.2002.02031.x>.
- Yang, Z., Sobocinski, K.L., Heatwole, D., Khangaonkar, T., Thom, R., Fuller, R., 2010. Hydrodynamic and ecological assessment of nearshore restoration: A modeling study. *Ecol. Model.* 221 (7), 1043–1053. <http://dx.doi.org/10.1016/j.ecolmodel.2009.07.011>.